2021 American Control Conference (ACC)
New Orleans, USA, May 25-28, 2021

# Sampled-Data Output-Feedback Model Predictive Control of Nonlinear Plants Using Online Linear System Identification

Tam W. Nguyen[1], Ilya V. Kolmanovsky[2], Dennis S. Bernstein[2]

*Abstract*— **In this paper, sampled-data output-feedback model predictive control (MPC) with online identification is used to control nonlinear continuous-time plants. Using a linear model structure for system identification, the paper provides a numerical investigation of the domain of attraction of MPC. Three examples are considered within the context of sampled-data control, namely, the second-order Duffing oscillator with a single measurement, the fourth-order ball-and-beam system with two measurements, and the sixth-order circular restricted three-body problem with three position measurements.**

## I. Introduction

Model predictive control (MPC) uses receding horizon optimization to achieve command following and stabilization while enforcing state and control constraints. MPC is one of the most widely studied techniques of modern control [1], [2], and a recent survey [3] suggests that it has a strong potential for practical impact in an increasing number of applications, for example, [4]–[6].

Since MPC is prediction-based, the plant model is crucial for ensuring closed-loop performance. Most versions of MPC are based on linear models [7]–[10], which are often obtained by linearizing a nonlinear model around an operating point. Not surprisingly, this approach is often effective only in a neighborhood of the operating point, and thus characterization of the domain of attraction is essential [11], [12].

Another way to deal with nonlinearities is to apply MPC directly to nonlinear models [13]–[15]. Unfortunately, the nonconvex nature of the problem significantly complicates the numerical optimization [16].

For realistic applications, MPC must be implemented in a sampled-data control architecture, which gives rise to intersample dynamics [17]–[19], and the possibility of constraint violation between samples.

In recent years, data-driven and learning-based MPC techniques [20]–[22] have been developed for plants that are not well modeled. Training-data-based MPC using neural networks is developed in [23], [24], while online data-driven policy adaptation, also known as data-enabled predictive control, is considered in [25], [26].

This paper applies output-feedback MPC with online identification (OFMPCOI) to nonlinear plants. OFMPCOI uses recursive least squares (RLS) with variable-rate forgetting to update a linear plant model online along with quadratic programming (QP) to perform the constrained, receding horizon optimization. An input-output model structure is used to facilitate output-feedback control without the need for a state estimator.

The present paper provides a numerical investigation of the application of OFMPCOI to nonlinear plants. This work is an extension of [27]–[29], which considered OFMPCOI for linear plants. In this paper, we apply OFMPCOI to several representative nonlinear plants based on online identification of a linear model. The goal of these examples is to investigate the ability of RLS-based identification with variable-rate forgetting to support OFMPCOI despite the mismatch between the nonlinear plant dynamics and the linear plant model.

This paper is organized as follows. First, a review of OFMPCOI is provided. The block observable canonical form of an input-output model is derived, the output and control constraints are defined, and the control architecture using RLS and QP is summarized. Next, we apply OFMPCOI to nonlinear plants and numerically investigate the controller through three examples, namely, the second-order Duffing oscillator with a single measurement, the fourth-order ball-and-beam system with two measurements, and the sixth-order circular restricted three-body problem with three position measurements.

**Notation.** The $n \times n$ identity matrix is denoted by $I_n$, the $m \times n$ matrix of ones by $1_{m\times n}$, the $m \times n$ matrix of zeros by $0_{m\times n}$, and the Kronecker product by $\otimes$.

## II. Review of OFMPCOI

The online system identification in OFMPCOI is based on an assumed MIMO input-output model of the form

$$y_k = -\sum_{i=1}^{n} F_i y_{k-i} + \sum_{i=0}^{n} G_i u_{k-i}, \tag{1}$$

where $k \geq 0$ is the time step, $n \geq 1$ is the data window, $u_k \in \mathbb{R}^m$ is the control, $y_k \in \mathbb{R}^p$ is the measurement, and $F_i \in \mathbb{R}^{p\times p}$ and $G_i \in \mathbb{R}^{p\times m}$ are model coefficients.

### A. Block Observable Canonical Form

Based on the structure of (1), for all $j \geq 1$, the $j$-step-ahead predicted output is given by

$$\begin{aligned} y_{j|k} = &-\sum_{i=1}^{j-1} \hat{F}_{i,k} y_{j-i|k} - \sum_{i=j}^{\hat{n}} \hat{F}_{i,k} y_{k+j-i} \\ &+ \sum_{i=0}^{j-1} \hat{G}_{i,k} u_{j-i|k} + \sum_{i=j}^{\hat{n}} \hat{G}_{i,k} u_{k+j-i}, \end{aligned} \tag{2}$$

where the first term is zero for $j = 1$, and the second and fourth terms are zero for $j > \hat{n}$. In (2), $u_{j|k} \in \mathbb{R}^m$ is the

[1]Department of Electrical and Electronic Engineering, University of Toyama, Toyama 930 8555, Japan
[2]Department of Aerospace Engineering, The University of Michigan, Ann Arbor, MI 48109, USA

$j$-step computed input, $\hat{F}_{i,k} \in \mathbb{R}^{p\times p}$ and $\hat{G}_{i,k} \in \mathbb{R}^{p\times m}$ are coefficient matrices estimated at step $k$, and $\hat{n} \geq 1$ is the data window used for estimation. Note that, in general, $\hat{n} \neq n$.

Next, based on [30], define the 1-step predicted state

$$x_{1|k} \triangleq \hat{A}_k \hat{x}_k + \hat{B}_k u_k, \tag{3}$$

where $\hat{x}_k \triangleq [\hat{x}_{1,k}^{\mathrm{T}} \ \cdots \ \hat{x}_{\hat{n},k}^{\mathrm{T}}]^{\mathrm{T}} \in \mathbb{R}^{\hat{n}p}$, and

$$\hat{x}_{1,k} \triangleq y_k - \hat{G}_{0,k} u_k, \tag{4}$$

$$\hat{x}_{i,k} \triangleq -\sum_{j=1}^{\hat{n}-i+1} \hat{F}_{i+j-1,k} y_{k-j} + \sum_{j=1}^{\hat{n}-i+1} \hat{G}_{i+j-1,k} u_{k-j}, \tag{5}$$

$$\hat{A}_k \triangleq \begin{bmatrix} -\hat{F}_{1,k} & I_p & \cdots & \cdots & 0_{p\times p} \\ \vdots & 0_{p\times p} & \ddots & & \vdots \\ \vdots & \vdots & \ddots & \ddots & 0_{p\times p} \\ \vdots & \vdots & & \ddots & I_p \\ -\hat{F}_{\hat{n},k} & 0_{p\times p} & \cdots & \cdots & 0_{p\times p} \end{bmatrix}, \hat{B}_k \triangleq \begin{bmatrix} \hat{G}_{1,k} - \hat{F}_{1,k}\hat{G}_{0,k} \\ \hat{G}_{2,k} - \hat{F}_{2,k}\hat{G}_{0,k} \\ \vdots \\ \hat{G}_{\hat{n},k} - \hat{F}_{\hat{n},k}\hat{G}_{0,k} \end{bmatrix}, \tag{6}$$

where $i = 2, \ldots, \hat{n}$. Note that (4) and (5) depend on past values of the measurement $y$ and control $u$ rather than the $j$-step predicted output $y_{j|k}$ given by (2) and the $j$-step computed input $u_{j|k}$ provided by QP. Hence, $x_{1|k}$ given by (3) is not necessarily equal to $\hat{x}_{k+1}$.

Defining the $j$-step predicted state

$$x_{j|k} \triangleq \hat{A}_k x_{j-1|k} + \hat{B}_k u_{j-1|k}, \quad j \geq 2, \tag{7}$$

the $j$-step predicted output (2) can be rewritten as

$$y_{j|k} = C x_{j|k} + \hat{D}_k u_{j|k}, \quad j \geq 2, \tag{8}$$

where $C \triangleq [I_p \ \ 0_{p\times p} \ \ \cdots \ \ 0_{p\times p}]$ and $\hat{D}_k \triangleq \hat{G}_{0,k}$. Note that the $j$-step prediction at step $k$ uses the current estimates $\hat{A}_k$, $\hat{B}_k$, and $\hat{D}_k$.

Next, defining

$$Y_{1|k,\ell} \triangleq \begin{bmatrix} y_{1|k} \\ \vdots \\ y_{\ell|k} \end{bmatrix} \in \mathbb{R}^{\ell p}, \quad U_{1|k,\ell} \triangleq \begin{bmatrix} u_{1|k} \\ \vdots \\ u_{\ell|k} \end{bmatrix} \in \mathbb{R}^{\ell m}, \tag{9}$$

it follows that

$$Y_{1|k,\ell} = \hat{\Gamma}_{k,\ell} x_{1|k} + \hat{T}_{k,\ell} U_{1|k,\ell}, \tag{10}$$

where $\hat{\Gamma}_{k,\ell} \in \mathbb{R}^{\ell p\times \hat{n}p}$ and $\hat{T}_{k,\ell} \in \mathbb{R}^{\ell p\times \ell m}$ are the observability and block-Toeplitz matrices

$$\hat{\Gamma}_{k,\ell} \triangleq \begin{bmatrix} C \\ C\hat{A}_k \\ \vdots \\ C\hat{A}_k^{\ell-1} \end{bmatrix}, \tag{11}$$

$$\hat{T}_{k,\ell} \triangleq \begin{bmatrix} \hat{D}_k & 0_{p\times m} & \cdots & \cdots & \cdots & \cdots & 0_{p\times m} \\ \hat{H}_{k,1} & \hat{D}_k & \cdots & \cdots & \cdots & \cdots & 0_{p\times m} \\ \hat{H}_{k,2} & \hat{H}_{k,1} & \hat{D}_k & \cdots & \cdots & \cdots & 0_{p\times m} \\ \hat{H}_{k,3} & \hat{H}_{k,2} & \hat{H}_{k,1} & \hat{D}_k & \cdots & \cdots & 0_{p\times m} \\ \hat{H}_{k,4} & \hat{H}_{k,3} & \hat{H}_{k,2} & \ddots & \ddots & & \vdots \\ \vdots & \vdots & \vdots & \ddots & \ddots & \ddots & 0_{p\times m} \\ \hat{H}_{k,\ell-1} & \hat{H}_{k,\ell-2} & \hat{H}_{k,\ell-3} & \cdots & \hat{H}_{k,2} & \hat{H}_{k,1} & \hat{D}_k \end{bmatrix}, \tag{12}$$

where, for all $i = 1, \ldots, \ell-1$, $\hat{H}_{k,i} \in \mathbb{R}^{p\times m}$ is defined by

$$\hat{H}_{k,i} \triangleq C\hat{A}_k^{i-1}\hat{B}_k. \tag{13}$$

### B. Tracking Output and Output Constraints

Define the tracking output $y_{\mathrm{t},k} \in \mathbb{R}^{p_{\mathrm{t}}}$ by

$$y_{\mathrm{t},k} \triangleq C_{\mathrm{t}} y_k, \tag{14}$$

where $C_{\mathrm{t}} \in \mathbb{R}^{p_{\mathrm{t}}\times p}$. The performance objective is to have $y_{\mathrm{t},k}$ follow a command trajectory $r_k \in \mathbb{R}^{p_{\mathrm{t}}}$, whose future values may or may not be known, and thus command preview may or may not be available. In addition to the performance objective, we define the constrained output $y_{\mathrm{c},k} \in \mathbb{R}^{p_{\mathrm{c}}}$ by

$$y_{\mathrm{c},k} \triangleq C_{\mathrm{c}} y_k, \tag{15}$$

where $C_{\mathrm{c}} \in \mathbb{R}^{p_{\mathrm{c}}\times p}$. The objective is to enforce the inequality constraint

$$\mathcal{C} y_{\mathrm{c},k} + \mathcal{D} \leq 0_{n_{\mathrm{c}}\times 1}, \tag{16}$$

where $\mathcal{C} \in \mathbb{R}^{n_{\mathrm{c}}\times p_{\mathrm{c}}}$ and $\mathcal{D} \in \mathbb{R}^{n_{\mathrm{c}}}$. Note that (16), where "$\leq$" is interpreted component-wise, defines a convex set.

### C. Control Constraints

The magnitude control constraint has the form

$$u_{\min} \leq u_k \leq u_{\max}, \tag{17}$$

where $u_{\min} \in \mathbb{R}^m$ is the vector of the minimum control magnitudes and $u_{\max} \in \mathbb{R}^m$ is the vector of maximum control magnitudes. In addition, the move-size control constraint has the form

$$\Delta u_{\min} \leq u_{k+1} - u_k \leq \Delta u_{\max}, \tag{18}$$

where $\Delta u_{\min} \in \mathbb{R}^m$ is the vector of minimum control move sizes and $\Delta u_{\max} \in \mathbb{R}^m$ is the vector of maximum control move sizes.

### D. Control Architecture

The control architecture combines output-feedback MPC with online linear system identification. In particular, these components are: (i) *identification*: the coefficients of a linear input-output model are estimated by RLS [31] to update the identified model for use by MPC, and (ii) *MPC*: the control input is updated by applying QP to the identified model.

*1) Online Identification:* For online identification, RLS is used to estimate the coefficients of an input-output model. For all $k \geq 0$, RLS minimizes the cumulative cost

$$J_k(\hat{\theta}) = \sum_{i=0}^{k} \frac{\rho_i}{\rho_k} z_i^{\mathrm{T}}(\hat{\theta}) z_i(\hat{\theta}) + \frac{1}{\rho_k}(\hat{\theta} - \theta_0)^{\mathrm{T}} P_0^{-1}(\hat{\theta} - \theta_0), \tag{19}$$

where $\rho_k \triangleq \prod_{j=0}^{k} \lambda_j^{-1} \in \mathbb{R}$, $\lambda_k \in (0, 1]$ is the forgetting factor, $P_0 \in \mathbb{R}^{[\hat{n}p(m+p)+mp]\times[\hat{n}p(m+p)+mp]}$ is positive definite, and $\theta_0 \in \mathbb{R}^{\hat{n}p(m+p)+mp]\times 1}$ is the initial estimate of the

coefficient vector. The performance variable $z_k(\hat{\theta}) \in \mathbb{R}^p$ is defined by

$$z_k(\hat{\theta}) \triangleq y_k + \sum_{i=1}^{\hat{n}} \hat{F}_i y_{k-i} - \sum_{i=0}^{\hat{n}} \hat{G}_i u_{k-i}, \tag{20}$$

where the vector of coefficients to be estimated $\hat{\theta} \in \mathbb{R}^{[\hat{n}p(m+p)+mp]\times 1}$ is defined by $\hat{\theta} \triangleq \operatorname{vec}[\hat{F}_1 \ \cdots \ \hat{F}_{\hat{n}} \ \ \hat{G}_0 \ \cdots \ \hat{G}_{\hat{n}}]^{\mathrm{T}}$. Defining the regressor matrix $\phi_k \in \mathbb{R}^{p\times[\hat{n}p(m+p)+mp]}$ by

$$\phi_k \triangleq I_p \otimes [-y_{k-1}^{\mathrm{T}} \ \cdots \ -y_{k-\hat{n}}^{\mathrm{T}} \ \ u_k^{\mathrm{T}} \ \cdots \ u_{k-\hat{n}}^{\mathrm{T}}], \tag{21}$$

it follows that (20) can be rewritten as

$$z_k(\hat{\theta}) = y_k - \phi_k \hat{\theta}. \tag{22}$$

Note that, with (22), the cost function (19) is strictly convex and quadratic, and thus has a unique global minimizer. The unique global minimizer $\theta_{k+1} \triangleq \operatorname{argmin}_{\hat{\theta}} J_k(\hat{\theta})$ is computed by RLS as:

$$L_k = \lambda_k^{-1} P_k, \tag{23}$$

$$P_{k+1} = L_k - L_k \phi_k^{\mathrm{T}} (I_p + \phi_k L_k \phi_k^{\mathrm{T}})^{-1} \phi_k L_k, \tag{24}$$

$$\theta_{k+1} = \theta_k + P_{k+1} \phi_k^{\mathrm{T}} (y_k - \phi_k \theta_k). \tag{25}$$

The time-dependent parameter $\lambda_k$ is the forgetting factor. In the case where $\lambda_k$ is constant, RLS uses constant-rate forgetting (CRF); otherwise, RLS uses variable-rate forgetting (VRF) [32]. For VRF, $\lambda_k$ is given by

$$\lambda_k = \frac{1}{1 + \eta g(z_{k-\tau_{\mathrm{d}}}, \ldots, z_k) \mathbf{1}[g(z_{k-\tau_{\mathrm{d}}}, \ldots, z_k)]}, \tag{26}$$

where $\mathbf{1}\colon \mathbb{R} \to \{0, 1\}$ is the unit step function, where $\mathbf{1}(x) = 0$ for $x < 0$ and $\mathbf{1}(x) = 1$ for $x \geq 0$, and

$$g(z_{k-\tau_{\mathrm{d}}}, \ldots, z_k) \triangleq \frac{\sqrt{1/\tau_{\mathrm{n}} \sum_{i=k-\tau_{\mathrm{n}}}^{k} z_i^{\mathrm{T}} z_i}}{\sqrt{1/\tau_{\mathrm{d}} \sum_{i=k-\tau_{\mathrm{d}}}^{k} z_i^{\mathrm{T}} z_i}} - 1. \tag{27}$$

In (26) and (27), $\eta \geq 0$ and $0 < \tau_{\mathrm{n}} < \tau_{\mathrm{d}}$ are numerator and denominator window lengths, respectively. Define $g(0, \ldots, 0) \triangleq 0$. If the sequence $z_{k-\tau_{\mathrm{d}}}, \ldots, z_k$ is zero-mean noise, then the numerator and denominator of (27) approximate the average standard deviation of the noise over the intervals $[k - \tau_{\mathrm{n}}, k]$ and $[k - \tau_{\mathrm{d}}, k]$, respectively.

*2) Control Update:* Let $\mathcal{R}_{k,\ell} \triangleq [r_{k+1}^{\mathrm{T}} \ \ldots r_{k+\ell}^{\mathrm{T}}]^{\mathrm{T}} \in \mathbb{R}^{\ell p_{\mathrm{t}}}$ be the vector of $\ell$ future commands, define $C_{\mathrm{t},\ell} \triangleq I_\ell \otimes C_{\mathrm{t}} \in \mathbb{R}^{\ell p_{\mathrm{t}} \times \ell p}$, let $Y_{\mathrm{t},1|k,\ell} \triangleq C_{\mathrm{t},\ell} Y_{1|k,\ell}$, where $Y_{1|k,\ell}$ is given by (10), be the $\ell$-step propagated tracking-output vector, define $\mathcal{C}_\ell \triangleq I_\ell \otimes (\mathcal{C} C_{\mathrm{c}}) \in \mathbb{R}^{\ell n_{\mathrm{c}} \times \ell p}$ and $\mathcal{D}_\ell \triangleq 1_{\ell\times 1} \otimes \mathcal{D} \in \mathbb{R}^{\ell n_{\mathrm{c}}}$, and define the sequence of differences of computed control inputs by $\Delta U_{1|k,\ell} \triangleq [(u_{1|k} - u_k)^{\mathrm{T}} \ (u_{2|k} - u_{1|k})^{\mathrm{T}} \ \cdots \ (u_{\ell|k} - u_{\ell-1|k})^{\mathrm{T}}]^{\mathrm{T}} \in \mathbb{R}^{\ell m}$. With this notation, QP-based MPC is given by:

$$\min_{U_{1|k,\ell}, \varepsilon} (Y_{\mathrm{t},1|k,\ell} - R_{k,\ell})^{\mathrm{T}} Q (Y_{\mathrm{t},1|k,\ell} - R_{k,\ell}) + (\Delta U_{1|k,\ell})^{\mathrm{T}} R \Delta U_{1|k,\ell} + \varepsilon^{\mathrm{T}} S \varepsilon \tag{28}$$

subject to

$$\mathcal{C}_\ell Y_{1|k,\ell} + \mathcal{D}_\ell \leq \varepsilon, \tag{29}$$

$$U_{\min} \leq U_{1|k,\ell} \leq U_{\max}, \tag{30}$$

$$\Delta U_{\min} \leq \Delta U_{1|k,\ell} \leq \Delta U_{\max}, \tag{31}$$

$$0_{\ell n_{\mathrm{c}} \times 1} \leq \varepsilon, \tag{32}$$

where $\varepsilon \in \mathbb{R}^{\ell n_{\mathrm{c}}}$ is the slack variable, $Q \triangleq \left[\begin{smallmatrix} \bar{Q} & 0_{p_{\mathrm{t}} \times p_{\mathrm{t}}} \\ 0_{p_{\mathrm{t}} \times p_{\mathrm{t}}} & \bar{P} \end{smallmatrix}\right] \in \mathbb{R}^{\ell p_{\mathrm{t}} \times \ell p_{\mathrm{t}}}$ is the positive-definite output weight, $\bar{Q} \in \mathbb{R}^{(\ell-1)p_{\mathrm{t}} \times (\ell-1)p_{\mathrm{t}}}$ is the positive-definite cost-to-go output weight, $\bar{P} \in \mathbb{R}^{p_{\mathrm{t}} \times p_{\mathrm{t}}}$ is the positive-definite terminal output weight, $R \in \mathbb{R}^{\ell m \times \ell m}$ is the positive-definite control weight, $S \in \mathbb{R}^{\ell n_{\mathrm{c}} \times \ell n_{\mathrm{c}}}$ is the positive-definite relaxation weight, $U_{\min} \triangleq 1_{\ell\times 1} \otimes u_{\min} \in \mathbb{R}^{\ell m}$, $U_{\max} \triangleq 1_{\ell\times 1} \otimes u_{\max} \in \mathbb{R}^{\ell m}$, $\Delta U_{\min} \triangleq 1_{\ell\times 1} \otimes \Delta u_{\min} \in \mathbb{R}^{\ell m}$, and $\Delta U_{\max} \triangleq 1_{\ell\times 1} \otimes \Delta u_{\max} \in \mathbb{R}^{\ell m}$. Since $R$ and $S$ are positive definite, (28)–(32) is a strictly convex optimization problem.

To solve (28)–(32), we use the accelerated dual gradient-projection algorithm [33], where the previously computed Lagrange multiplier is used to warmstart the solver at the next time instant. For real-time implementation, the control computed between $k$ and $k + 1$ is implemented at step $k + 1$. Identification and control do not commence until the regressor matrix $\phi_k$ given by (21) is populated with $\hat{n}$ measurements.

## III. OFMPCOI for Nonlinear Plants

In the sequel, we apply OFMPCOI to nonlinear plants represented by

$$\dot{x} = f(x, u, w), \tag{33}$$

$$y = g(x), \tag{34}$$

where $x \in \mathbb{R}^n$ is the state, $w \in \mathbb{R}^q$ is the unmatched disturbance, and $f : \mathbb{R}^n \times \mathbb{R}^m \to \mathbb{R}^n$ and $g : \mathbb{R}^n \to \mathbb{R}^p$ are nonlinear functions.

In all examples, we assume that the analog-to-digital conversion is an instantaneous sampler, and that the digital-to-analog conversion is a zero-order-hold (ZOH) device. OFMPCOI is run between samples, and the continuous-time dynamics are integrated by ode45. All commands are discrete-time signals, and all deterministic disturbances are discretized at the integration step size.

## IV. Numerical Examples

**Example 1.** *Duffing oscillator,* $n = 2$. The dynamics of the forced Duffing oscillator are given by

$$\dot{x}_1 = x_2, \tag{35}$$

$$\dot{x}_2 = -\alpha x_1^3 + \beta x_1 - \delta x_2 + u, \tag{36}$$

where $\alpha \geq 0$, $\beta \geq 0$, and $\delta \geq 0$. Note that, for $\alpha > 0$ and $\beta > 0$, the uncontrolled system has equilibria at $(0, 0)$ and $(\pm\sqrt{\beta/\alpha}, 0)$. Assume that the position $x_1$ is measured and serves as the tracking output, that is, $y = y_{\mathrm{t}} = x_1$. No output constraint is considered in this example. Let $\alpha = 1.5$, $\beta = 1$, and $\delta = 0.8$. The control constraints are given by

$u_{\max} = \Delta u_{\max} = 10$, and $u_{\min} = \Delta u_{\min} = -10$. The data are sampled with sample period $T_{\rm s} = 0.1$ s. The parameters of OFMPCOI are $\hat{n} = n = 2$, $\ell = 20$, $\bar{Q} = 40I_{\ell-1}$, $\bar{P} = 40$, $R = I_\ell$, and $P_0 = 10^3 I_{\hat{n}p(p+m)-mp}$, and the initial model of OFMPCOI is strictly proper and FIR, that is, $\theta_0 = [0_{1\times(\hat{n}p(p+m)-mp)}\ 1_{1\times mp}]^{\rm T}$. This example does not consider command preview, that is, $R_{k,\ell} = 1_{\ell\times 1} \otimes r_k$. The parameters of VRF are $\eta = 0.9$, $\tau_{\rm n} = 20$, and $\tau_{\rm d} = 40$.

**Characterization of the domain of attraction of the origin.** Consider the stabilization case $r_k \equiv 0$, where CRF with $\lambda = 0.9$ is used. Let $\bar{x} \in \mathbb{R}^n$ be an equilibrium point to be investigated, let $\gamma(\bar{x}, \rho) \subset \mathbb{R}^n$ be the domain of investigation, which is a ball of radius $\rho > 0$ centered at $\bar{x}$, and let $\mathcal{D}_\gamma(\bar{x}, \rho) \subseteq \gamma(\bar{x}, \rho)$ be the local domain of attraction of $\bar{x}$. Given $\bar{x} \in \mathbb{R}^n$ and $\rho > 0$, we numerically approximate the true local domain of attraction by computing the discrete set $\tilde{\mathcal{D}}_\gamma(\bar{x}, \rho)$ such that $\tilde{\mathcal{D}}_\gamma(\bar{x}, \rho) \approx \mathcal{D}_\gamma(\bar{x}, \rho)$. To do so, we run $n_{\rm s}$ simulations of length $T_{\rm exp} > 0$ using a grid of initial conditions $\mathcal{G} = \{x_{0,i} \colon x_{0,i} \in \gamma(\bar{x}, \rho),\ i, \ldots, n_{\rm s}\}$, and, for each simulation, we reject the initial condition $x_{0,i}$ for which, from a specific point in time until the end of the simulation, the maximum error norm is above a specified threshold, that is, $\max_{T_{\rm test} \le t \le T_{\rm exp}} \|x(t) - \bar{x}\| > \epsilon_{\max}$, where $0 < T_{\rm test} < T_{\rm exp}$ and $\epsilon_{\max} > 0$ is sufficiently small. Accordingly, we construct the approximate local domain of attraction $\tilde{\mathcal{D}}_\gamma(\bar{x}, \rho)$ by accumulating the acceptable initial conditions $x_{0,i}$. Figure 1 shows the approximate local domain of attraction $\tilde{\mathcal{D}}_\gamma(\bar{x}, \rho)$ and the corresponding responses of OFMPCOI using a grid of 317 initial conditions satisfying $x(0) \in \tilde{\mathcal{D}}_\gamma(\bar{x}, \rho)$, $\bar{x} = [0\ 0]^{\rm T}$, $\rho = 100$, $\epsilon_{\max} = 10^{-2}$, $T_{\rm test} = 40$ s, and $T_{\rm exp} = 50$ s. Note that the approximate local domain of attraction is close to the domain of investigation, that is, $\tilde{\mathcal{D}}_\gamma(\bar{x}, \rho) \approx \gamma(\bar{x}, \rho)$.

**Example 2.** *Ball-and-beam system,* $n = 4$. Define $x = [x_1\ x_2\ x_3\ x_4]^{\rm T} \triangleq [q\ \dot{q}\ \theta\ \dot{\theta}]^{\rm T}$ as the state vector, where $q \in \mathbb{R}$ is the position of the ball, and $\theta \in [-\pi, \pi)$ is the angle of the beam relative to the horizontal. Let $u \in \mathbb{R}$ be the control moment applied to the center of the beam, $m_{\rm b} > 0$ be the mass of the ball, $J > 0$ be the moment of inertia of the beam, and $g > 0$ be the gravity acceleration. The dynamics of the ball-and-beam system are represented by the following model:

$$\dot{x} = \begin{bmatrix} x_2 \\ x_1 x_4^2 - g\sin(x_3) \\ x_4 \\ -\frac{m_{\rm b} x_1}{m_{\rm b} x_1^2 + J}[2x_2x_4 + g\cos(x_3)] \end{bmatrix} + \begin{bmatrix} 0 \\ 0 \\ 0 \\ \frac{1}{m_{\rm b} x_1^2 + J} \end{bmatrix} u. \quad (37)$$

Assume that the position of the ball $q$ and the angle of the beam $\theta$ are measured, and that the tracking output is the position of the ball $q$, that is, $y = [q\ \theta]^{\rm T}$ and $y_{\rm t} = q$. The output constraints are $-1 \le q \le 1$ and $-\pi/4 \le \theta \le \pi/4$. The linearization of (37) at the origin is given by

$$\dot{x} = \begin{bmatrix} 0 & 1 & 0 & 0 \\ 0 & 0 & -g & 0 \\ 0 & 0 & 0 & 1 \\ -m_{\rm b} g J^{-1} & 0 & 0 & 0 \end{bmatrix} x + \begin{bmatrix} 0 \\ 0 \\ 0 \\ J^{-1} \end{bmatrix} u, \quad (38)$$

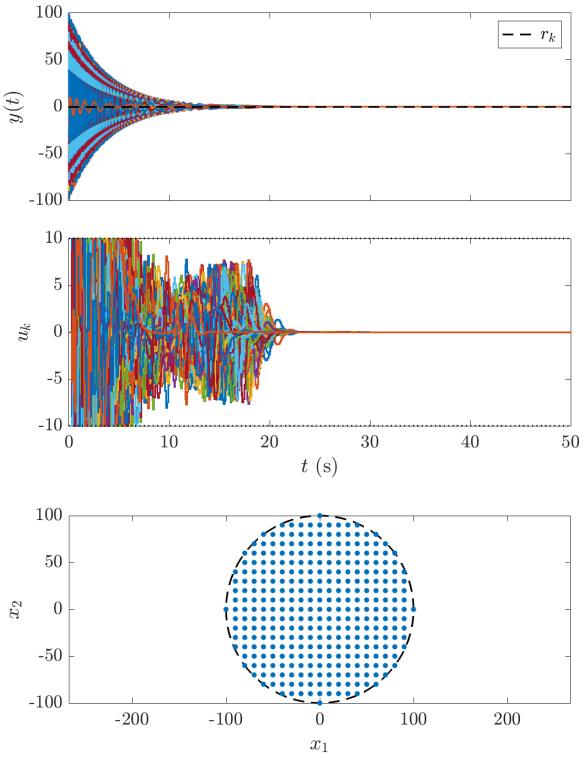


Fig. 1: Example 1. Stabilization of the Duffing oscillator (35), (36) using CRF with $\lambda = 0.9$ for a grid of 317 initial conditions satisfying $x(0) \in \tilde{\mathcal{D}}_\gamma(\bar{x}, \rho)$, $\bar{x} = [0\ 0]^{\rm T}$, $\rho = 100$, $\epsilon_{\max} = 10^{-2}$, $T_{\rm test} = 40$ s, and $T_{\rm exp} = 50$ s. The three first plots show the responses of OFMPCOI, and the bottom-most plot shows the approximate local domain of attraction $\tilde{\mathcal{D}}_\gamma(\bar{x}, \rho)$, which is approximately the domain of investigation, that is, $\tilde{\mathcal{D}}_\gamma(\bar{x}, \rho) \approx \gamma(\bar{x}, \rho)$.

where, for $T_{\rm s} = 0.1$ s, $g = 9.81$ m/s$^2$, $m = 0.1$ kg, and $J = 0.3$ kg.m$^2$, the discrete-time transfer functions from $u$ to $q$ and from $u$ to $\theta$ using ZOH are given by

$$G_1(z) = \frac{-(1.363z^3 + 14.99z^2 + 14.99z + 1.363)\mathrm{e}^{-4}}{z^4 - 4.001z^3 + 5.998z^2 - 4.001z + 1}, \quad (39)$$

$$G_2(z) = \frac{1.667\mathrm{e}^{-2}(z^3 - z^2 - z + 1)}{z^4 - 4.001z^3 + 5.998z^2 - 4.001z + 1}, \quad (40)$$

respectively. The control constraints are $u_{\max} = 1$ Nm, $u_{\min} = -1$ Nm, $\Delta u_{\max} = 0.5$ Nm, and $\Delta u_{\min} = -0.5$ Nm. The parameters of OFMPCOI are $\ell = 20$, $\bar{Q} = 40I_{\ell-1}$, $\bar{P} = 40$, $R = I_\ell$, and $S = 5 \times 10^3 I_4$. This example does not consider command preview, that is, $R_{k,\ell} = 1_{\ell\times 1} \otimes r_k$. The parameters of VRF are $\eta = 0.9$, $\tau_{\rm n} = 20$, and $\tau_{\rm d} = 40$.

**Characterization of the domain of attraction of the origin.** Consider the stabilization case $r_k \equiv 0$ for $\hat{n} = 2 < n = 4$ with VRF. The initial model used by OFMPCOI is close to (39), (40), and has $\theta_0 = [-2.00\ 0.43\ 1.00\ -0.38\ 0.00\ 0.09\ 0.00\ -1.80\ 0.00\ 0.77\ 0.03\ 0.01]^{\rm T}$. Similarly to Example 1, we compute the approximate local domain of attraction $\tilde{\mathcal{D}}_\gamma(\bar{x}, \rho)$ using a grid of initial conditions satisfying $x(0) \in \mathcal{D}_\gamma(\bar{x}, \rho)$, $\bar{x} = [0\ 0\ 0\ 0]^{\rm T}$, $\rho = 0.5$, $\epsilon_{\max} = 10^{-2}$, $T_{\rm test} = 20$ s, and $T_{\rm exp} = 25$ s. For $\dot{\theta}(0) = 0$ and a grid of 4169 initial conditions, Figure 2 compares the approximate local domain of attraction using $P_0 = 10^3 I_{\hat{n}p(p+m)-mp}$ and $P_0 = I_{\hat{n}p(p+m)-mp}$, and shows the corresponding responses of OFMPCOI. It is shown that, in contrast to

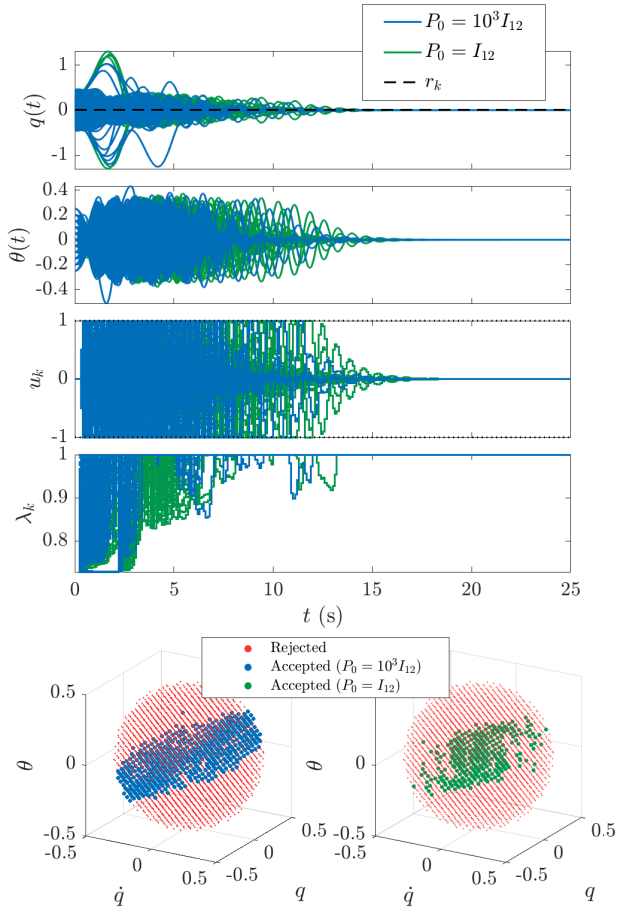


Fig. 2: Example 2. Stabilization of the ball-and-beam system (37) for $\hat{n} = 2 < n = 4$ with VRF. For $\dot{\theta}(0) = 0$ and a grid of 4169 initial conditions, the first four plots compare the converged responses of OFMPCOI using $P_0 = 10^3 I_{\hat{n}p(p+m)-mp}$ and $P_0 = I_{\hat{n}p(p+m)-mp}$, and the bottom-most plot shows the corresponding approximate local domains of attraction $\hat{\mathcal{D}}_\gamma(\bar{x}, \rho)$ for $\bar{x} = [0\ 0\ 0\ 0]^{\mathrm{T}}$, $\rho = 0.5$, $\epsilon_{\max} = 10^{-2}$, $T_{\mathrm{test}} = 20$ s, and $T_{\mathrm{exp}} = 25$ s. In contrast to Example 1, neither of the approximate local domains of attraction includes all of initial conditions in the domain of investigation $\gamma(\bar{x}, \rho)$. Furthermore, the approximate local domain of attraction with $P_0 = 10^3 I_{\hat{n}p(p+m)-mp}$ contains more points than the one with $P_0 = I_{\hat{n}p(p+m)-mp}$, where 719 and 329 initial conditions are accepted, respectively.

Example 1, neither of the approximate local domains of attraction includes all of initial conditions in the domain of investigation $\gamma(\bar{x}, \rho)$. Furthermore, the approximate local domain of attraction with $P_0 = 10^3 I_{\hat{n}p(p+m)-mp}$ contains more points than the one with $P_0 = I_{\hat{n}p(p+m)-mp}$, where 719 and 329 initial conditions are admissible, respectively.

**Example 3.** *Circular restricted three-body problem,* $n = 6$. Consider a system composed of three point-masses [34], [35], which represent the celestial body 1, the celestial body 2, and the spacecraft. Let $m_1 > 0$ and $m_2 > 0$ be the masses of celestial body 1 and celestial body 2, respectively, $\delta > 0$ be the distance between the two celestial bodies, and $\chi = \frac{m_1}{m_1+m_2}$. Assume that the celestial bodies rotate at the constant rate $\omega = \sqrt{\frac{G(m_1+m_2)}{\delta^3}}$ about their center of mass, where $G$ is the gravitational constant. The spacecraft dynamics are modeled as

$$\ddot{x} = 2\dot{y} + x - \frac{(1-\chi)(x+\chi)}{r_1^3} - \frac{\chi(x-1+\chi)}{r_2^3} + \frac{F_x}{m_{\mathrm{s}}\omega^2\delta}, \quad (41)$$

$$\ddot{y} = -2\dot{x} + y - \frac{(1-\chi)y}{r_1^3} - \frac{\chi y}{r_2^3} + \frac{F_y}{m_{\mathrm{s}}\omega^2\delta}, \quad (42)$$

$$\ddot{z} = -\frac{(1-\chi)z}{r_1^3} - \frac{\chi z}{r_2^3} + \frac{F_z}{m_{\mathrm{s}}\omega^2\delta}, \quad (43)$$

where $m_{\mathrm{s}} > 0$ is the mass of the spacecraft, $m_{\mathrm{s}} \ll m_1$, $m_{\mathrm{s}} \ll m_2$, $F_x \in \mathbb{R}$, $F_y \in \mathbb{R}$, and $F_z \in \mathbb{R}$ are the $x$-, $y$-, and $z$-force acting on the spacecraft resolved in the body-fixed frame, respectively, and $r_1 = \sqrt{(x+\chi)^2 + y^2 + z^2}$ and $r_2 = \sqrt{(x-1+\chi)^2 + y^2 + z^2}$. Note that, in (41)–(43), the force is in kN, one unit of time is $\omega^{-1}$ s, and one unit of distance is $\delta$ km. Let $\chi = 1.215059 \times 10^{-2}$, $\omega = 2\pi/(655.728 \times 3600)$ rad/s, $\delta = 384400$ km, and $m_{\mathrm{s}} = 2000$ kg. Assume that the control input is $u_k = [F_x\ F_y\ F_z]^T$, and that the output is the spacecraft position, which serves as the tracking output, that is, $y = [x\ y\ z]^{\mathrm{T}}$, and $y_{\mathrm{t}} = y$. No output constraint is considered in this example.

The data are sampled with $T_{\mathrm{s}} = 10^{-2}\omega^{-1}$ s. The initial model of OFMPCOI uses $\theta_0 = [0_{1\times(\hat{n}p(p+m)-mp)}\ 1_{1\times mp}]^{\mathrm{T}}$. Let $u_{\max} = 1$ kN, $u_{\min} = -1$ kN, $\Delta u_{\min} = -0.5$ kN, and $\Delta u_{\max} = 0.5$ kN. The parameters are $\ell = 20$, $\bar{Q} = 40I_3 \otimes I_{\ell-1}$, $\bar{P} = 40I_3$, $R = I_3 \otimes I_\ell$, $P_0 = 10^3 I_{\hat{n}p(p+m)-mp}$, and $\hat{n} = 2$. OFMPCOI uses VRF with $\eta = 0.1$, $\tau_{\mathrm{n}} = 5$, and $\tau_{\mathrm{d}} = 10$, and has preview on the reference trajectory, which is a pre-computed halo orbit.

For a grid of 49 initial conditions in the neighborhood of a point on the halo orbit, Figure 3 shows the three-dimensional trajectories of the spacecraft, where $T = 2.047\omega^{-1}$ s is one orbit period. It is shown that, for each initial condition, a poor initial model causes a large transient in the first two orbit periods. Afterwards, however, the spacecraft approaches the halo orbit.

## V. Conclusions and Future Research

Output-feedback model predictive control with online identification (OFMPCOI) was applied to nonlinear plants. The goal of this numerical investigation was to determine the domain of attraction resulting from the use of a linear model of a nonlinear plant. For the fourth-order ball-and-beam system with two measurements, the domain of attraction was found to be a limited subset of the tested initial conditions. However, since this system is unstable, the domain of attraction is necessarily limited by the control saturation. Future research will examine the effect of control saturation on the domain of attraction as distinct from the effect of the linear model structure. Finally, it will be interesting to apply this technique to nonlinear plants that cannot be stabilized by continuous controllers [19].

## VI. Acknowledgments

This research was supported by ONR under BRC grant N00014-18-1-2211.

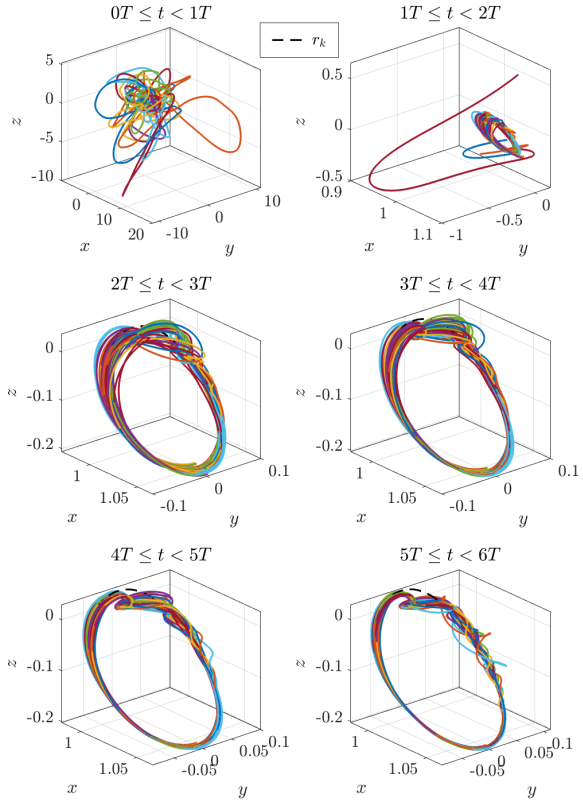


Fig. 3: Example 3. Three-dimensional trajectories of the spacecraft for the circular restricted three-body problem (41)–(43) using a grid of 49 initial conditions, where $T = 2.047\omega^{-1}$ s is one orbit period. Note that, for each initial condition, after a large transient in the first two orbit periods, the position of the spacecraft approaches the reference.

## REFERENCES


[1] J. B. Rawlings, D. Q. Mayne, and M. M. Diehl, *Model Predictive Control: Theory, Computation, and Design*, 2nd ed. Nob Hill Publishing, LLC, 2017.

[2] S. V. Raković and W. S. Levine, *Handbook of Model Predictive Control*. Birkhäuser, 2019.

[3] T. Samad, M. Bauer, S. Bortoffc, S. Di Cairano, L. Fagiano, P. F. Odgaard, R. R. Rhinehart, R. Sánchez-Peña, A. Serbezov, F. Ankersen, P. Goupil, B. Grosman, M. Heertjes, I. Mareels, and R. Sosseh, "Industry engagement with control research: Perspective and messages," *Ann. Rev. Contr.*, vol. 49, pp. 1–14, 2020.

[4] S. Koch, M. Ponikvar, M. Steinberger, and M. Horn, "Model predictive temperature control of a distribution system for chemicals," in *Dynamics and Control of Advanced Structures and Machines*. Springer, 2017, pp. 109–117.

[5] S. Di Cairano and I. V. Kolmanovsky, "Automotive applications of model predictive control," in *Handbook of Model Predictive Control*. Springer, 2019, pp. 493–527.

[6] U. Eren, A. Prach, B. B. Koçer, S. V. Raković, E. Kayacan, and B. Açıkmeşe, "Model predictive control in aerospace systems: Current state and opportunities," *Journal of Guidance, Control, and Dynamics*, vol. 40, no. 7, pp. 1541–1566, 2017.

[7] K. R. Muske and J. B. Rawlings, "Model predictive control with linear models," *AIChE Journal*, vol. 39, no. 2, pp. 262–287, 1993.

[8] A. Bemporad, "Model predictive control design: New trends and tools," in *Proc. Conf. Dec. Contr.*, 2006, pp. 6678–6683.

[9] A. Bemporad and P. Patrinos, "Simple and certifiable quadratic programming algorithms for embedded linear model predictive control," *IFAC Proc. Vol.*, vol. 45, no. 17, pp. 14–20, 2012.

[10] L. A. Alvarez and D. Odloak, "Robust integration of real time optimization with linear model predictive control," *Computers & Chemical Engineering*, vol. 34, no. 12, pp. 1937–1944, 2010.

[11] D. Limon, T. Alamo, and E. F. Camacho, "Enlarging the domain of attraction of MPC controllers," *Automatica*, vol. 41, no. 4, pp. 629–635, 2005.

[12] S. Grammatico and G. Pannocchia, "Achieving a large domain of attraction with short-horizon linear MPC via polyhedral lyapunov functions," in *Proc. Eur. Contr. Conf.*, 2013, pp. 1059–1064.

[13] M. A. Henson, "Nonlinear model predictive control: current status and future directions," *Computers & Chemical Engineering*, vol. 23, no. 2, pp. 187–202, 1998.

[14] F. Allgöwer and A. Zheng, *Nonlinear Model Predictive Control*. Birkhäuser, 2012.

[15] L. Magni, D. M. Raimondo, and F. Allgöwer, *Nonlinear Model Predictive Control*. Springer, 2009.

[16] D. Mayne, "Nonlinear model predictive control: Challenges and opportunities," in *Nonlinear Model Predictive Control*. Springer, 2000, pp. 23–44.

[17] F. Fontes, S. Raković, and I. Kolmanovsky, "Rigid tube model predictive control for linear sampled–data systems," *IFAC-PapersOnLine*, vol. 50, no. 1, pp. 9840 – 9845, 2017, 20th IFAC World Congress.

[18] R. Findeisen, L. Imsland, F. Allgöwer, and B. Foss, "Towards a sampled-data theory for nonlinear model predictive control," in *New Trends in Nonlinear Dynamics and Control and their Applications*, W. Kang, C. Borges, and M. Xiao, Eds. Berlin, Heidelberg: Springer, 2003, pp. 295–311.

[19] F. Fontes, "Discontinuous feedbacks, discontinuous optimal controls, and continuous-time model predictive control," *International Journal of Robust and Nonlinear Control*, vol. 13, no. 3-4, pp. 191–209, 2003.

[20] D. Limon, J. Calliess, and J. M. Maciejowski, "Learning-based nonlinear model predictive control," *IFAC-PapersOnLine*, vol. 50, no. 1, pp. 7769–7776, 2017.

[21] M. Maiworm, D. Limon, J. M. Manzano, and R. Findeisen, "Stability of Gaussian process learning based output feedback model predictive control," *IFAC-PapersOnLine*, vol. 51, no. 20, pp. 455–461, 2018.

[22] L. Hewing, K. P. Wabersich, M. Menner, and M. N. Zeilinger, "Learning-based model predictive control: Toward safe learning in control," *Annual Review of Control, Robotics, and Autonomous Systems*, vol. 3, pp. 269–296, 2020.

[23] B. M. Åkesson and H. T. Toivonen, "A neural network model predictive controller," *J. Proc. Contr.*, vol. 16, pp. 937–946, 2006.

[24] R. Hedjar, "Adaptive neural network model predictive control," *International Journal of Innovative Computing, Information and Control*, vol. 9, no. 3, pp. 1245–1257, 2013.

[25] J. Coulson, J. Lygeros, and F. Dörfler, "Data-enabled predictive control: In the shallows of the DeePC," in *Proc. Eur. Contr. Conf.*, 2019, pp. 307–312.

[26] S. Baros, C.-Y. Chang, G. E. Colon-Reyes, and A. Bernstein, "Online data-enabled predictive control," *arXiv:2003.03866*, 2020.

[27] T. W. Nguyen, S. A. Ul Islam, A. L. Bruce, A. Goel, D. S. Bernstein, and I. V. Kolmanovsky, "Output-feedback RLS-based model predictive control," in *Proc. Amer. Contr. Conf.*, 2020, pp. 2395–2400.

[28] N. Mohseni, T. W. Nguyen, S. A. Ul Islam, I. V. Kolmanovsky, and D. S. Bernstein, "Active noise control for harmonic and broadband disturbances using RLS-based model predictive control," in *Proc. Amer. Contr. Conf.*, 2020, pp. 1393–1398.

[29] T. W. Nguyen, S. A. U. Islam, D. S. Bernstein, and I. V. Kolmanovsky, "Output-feedback model predictive control with online identification," 2020. [Online]. Available: https://arxiv.org/abs/2009.10631

[30] J. W. Polderman, "A state space approach to the problem of adaptive pole assignment," *Mathematics of Control, Signals and Systems*, vol. 2, no. 1, pp. 71–94, 1989.

[31] S. A. U. Islam and D. S. Bernstein, "Recursive least squares for real-time implementation," *IEEE Contr. Sys. Mag.*, vol. 39, no. 3, pp. 82–85, 2019.

[32] A. L. Bruce, A. Goel, and D. S. Bernstein, "Convergence and consistency of recursive least squares with variable-rate forgetting," *Automatica*, vol. 119, p. 109052, 2020.

[33] P. Patrinos and A. Bemporad, "An accelerated dual gradient-projection algorithm for embedded linear model predictive control," *IEEE Trans. Autom. Contr.*, vol. 59, no. 1, pp. 18–33, 2014.

[34] W. S. Koon, M. W. Lo, J. E. Marsden, and S. D. Ross, *Dynamical systems, the three-body problem and space mission design*. Marsden Books, 2008.

[35] A. W. Berning Jr., D. Liao-McPherson, A. Girard, and I. Kolmanovsky, "Suboptimal nonlinear model predictive control strategies for tracking near rectilinear halo orbits," 2020. [Online]. Available: https://arxiv.org/abs/2008.09240